MOLECULAR AND CELLULAR BIOLOGY, Dec. 2005, p. 10261–10272 Vol. 25, No. 23
0270-7306/05/$08.00+0 doi:10.1128/MCB.25.23.10261–10272.2005

Muscle-Specific Loss of Apoptosis-Inducing Factor Leads to Mitochondrial Dysfunction, Skeletal Muscle Atrophy, and Dilated Cardiomyopathy

Nicholas Joza,[1,2,3]* Gavin Y. Oudit,[4] Doris Brown,[5] Paule Bénit,[6] Zamaneh Kassiri,[3] Nicola Vahsen,[7] Loralyn Benoit,[2] Mikin M. Patel,[4] Karin Nowikovsky,[8] Anne Vassault,[7] Peter H. Backx,[4] Teiji Wada,[1] Guido Kroemer,[7] Pierre Rustin,[6] and Josef M. Penninger[1,2,3]*

Institute of Molecular Biotechnology of the Austrian Academy of Sciences, Dr. Bohrgasse 7, 1030 Vienna, Austria[1]; Departments of Immunology[2] and Medical Biophysics,[3] University of Toronto, Toronto, Ontario, Canada; Departments of Physiology and Medicine, Division of Cardiology, University Health Network, and Heart and Stroke Richard Lewar Centre, University of Toronto, Toronto, Ontario, Canada[4]; Department of Anatomy, University of California at San Francisco, San Francisco, California 94143-2711[5]; INSERM U676, Hopital Robert Debre, 75019 Paris, France[6]; Centre National de la Recherche Scientifique, UMR1599, Institut Gustave Roussy, Villejuif, France[7]; and Max F. Perutz Laboratories, Departments of Microbiology and Genetics, University of Vienna, Campus Vienna Biocenter, A-1030 Vienna, Austria[8]

Received 16 August 2005/Accepted 17 August 2005

Cardiac and skeletal muscle critically depend on mitochondrial energy metabolism for their normal function. Recently, we showed that apoptosis-inducing factor (AIF), a mitochondrial protein implicated in programmed cell death, plays a role in mitochondrial respiration. However, the in vivo consequences of AIF-regulated mitochondrial respiration resulting from a loss-of-function mutation in *Aif* are not known. Here, we report tissue-specific deletion of *Aif* in the mouse. Mice in which *Aif* has been inactivated specifically in cardiac and skeletal muscle exhibit impaired activity and protein expression of respiratory chain complex I. Mutant animals develop severe dilated cardiomyopathy, heart failure, and skeletal muscle atrophy accompanied by lactic acidemia consistent with defects in the mitochondrial respiratory chain. Isolated hearts from mutant animals exhibit poor contractile performance in response to a respiratory chain-dependent energy substrate, but not in response to glucose, supporting the notion that impaired heart function in mutant animals results from defective mitochondrial energy metabolism. These data provide genetic proof that the previously defined cell death promoter AIF has a second essential function in mitochondrial respiration and aerobic energy metabolism required for normal heart function and skeletal muscle homeostasis.

In animals, the growth and maintenance of tissues absolutely depend on energy metabolism, which is met principally through mitochondrial oxidative phosphorylation (OXPHOS). OXPHOS is a complex biochemical process in which electrons generated from the catabolism of energy substrates flow through a series of catalysts known as the mitochondrial respiratory chain; the free energy liberated from this oxidative process drives formation of an electrochemical potential difference across the inner mitochondrial membrane which is utilized to generate energy for the cell in the form of ATP. Defects in OXPHOS and mitochondrial energy metabolism are implicated in a wide spectrum of human disorders, including myopathies and cardiomyopathies, diabetes mellitus, neurodegenerative illnesses such as Alzheimer's disease, and aging (5, 9, 39, 40).

In addition to functioning as the powerhouses of the cell, mitochondria are essential to a cell's suicide machinery, initiating apoptosis through the release of potentially toxic proteins from the mitochondrial intermembrane space into the cytosol (7, 14). One of these mitochondrial proteins is the hemoprotein cytochrome *c*, whose role in healthy cells is to shuttle electrons from complex III to IV of the respiratory chain. However, during apoptosis, cytosolic cytochrome *c* stimulates formation of the apoptosome, a caspase-activating complex (4). In addition to cytochrome *c*, other apoptotic effectors are released from mitochondria, including the serine protease Omi/Htra2, Smac/Diablo, endonuclease G, and apoptosis-inducing factor (AIF) (7).

AIF is an evolutionarily conserved flavoprotein closely associated with the inner mitochondrial membrane (36). In several cellular contexts in species including yeast, *Caenorhabditis elegans*, and in mammals, AIF has been implicated as a cell death-promoting molecule that translocates from mitochondria to the nucleus after proapoptotic signals and mediates chromatin condensation and large-scale DNA fragmentation (18, 25, 36, 42, 43). In addition to its cell death effector functions, AIF has been shown to be required for cell survival and has been suggested to function as a scavenger of reactive oxygen species (ROS) (19). The Harlequin (*Hq*) mouse mutant, which manifests an ~80% reduction in AIF protein levels due to a proviral insertion in the first intron of the *Aif* gene, exhibits progressive cerebellar and retinal degeneration associated with increased levels of oxidative stress markers (20). Recently, it has been shown that cardiomyocytes from *Hq* mice were sen-

* Corresponding author. Mailing address: Institute of Molecular Biotechnology of the Austrian Academy of Sciences, Dr. Bohrgasse 3-5, 1030 Vienna, Austria. Phone: (43-1)79730454. Fax: (43-1) 79730459. E-mail for Nicholas Joza: nicholas.joza@imba.oeaw.ac.at. E-mail for Josef M. Penninger: josef.penninger@imba.oeaw.ac.at.

sitized to oxidative stress-induced cell death, and *Hq* hearts displayed more severe ischemic damage compared to wild-type hearts after acute ischemia/reperfusion injury (38). In addition, we have reported a requirement for AIF in OXPHOS and for the assembly and/or stabilization of respiratory complex I (37). It remains unclear, however, whether AIF functions primarily in scavenging cellular ROS or controlling OXPHOS function. Moreover, the in vivo consequences of a targeted *Aif* null mutation on mouse embryonic development and in adult tissues have not been explored.

Here we report the targeted disruption of *Aif* in mice. Loss of AIF expression during embryogenesis results in embryonic growth retardation and death during midgestation. Mice lacking AIF in muscle develop severe dilated cardiomyopathy and skeletal muscle atrophy, associated with a severe defect in respiratory chain complex I activity, significantly reduced levels of complex I proteins, and metabolic alterations that resemble human mitochondriopathies. We demonstrate that AIF-regulated mitochondrial respiration and energy homeostasis are critical for normal heart function and skeletal muscle maintenance.

MATERIALS AND METHODS

Generation of mice carrying the *Aif* conditional allele. The targeting vector for producing the *Aif*^{flox} allele consisted of a 1.1-kb fragment of *Aif* genomic DNA containing exon 7 with *loxP* sequences inserted in the introns on either side of it, an ~10-kb fragment spanning exons 8 to 14, and a 600-bp fragment 5′ of exon 7, cloned into a targeting vector backbone containing PGKneo and DTA-positive and -negative selection cassettes, respectively. The linearized construct was electroporated into E14Tg2a.4 embryonic stem (ES) cells, derived from the 129/Ola strain (16). Approximately 1 in 100 ES cell clones were identified as correctly targeted by genomic Southern blotting. Five such clones were transiently transfected with the pCAGGs-FLPe vector (3) to excise the *frt*-flanked PGKneo cassette. Subclones that no longer contained the PGKneo cassette as determined by Southern blot were injected into C57BL/6 blastocysts. Chimeric mice from two independent clones transmitted the mutant allele through the germ line. Mice carrying the *Aif*^{flox} allele were backcrossed two to four times to C57BL/6 mice before generating the Mck-*cre*; *Aif*^{flox}/Y animals. It should be noted that we observed similar phenotypes in Mck-*cre*; *Aif*^{flox}/Y males and Mck-*cre*; *Aif*-$^{flox/flox}$ females. For mouse genotyping, genomic DNA from mouse tails was isolated and amplified by PCR with three primers: P1, 5′-GAATCTGGAATA TGGCACAGAGG-3′; P2, 5′-GGATTAAAGGCATGTGCCAACACG-3′; and P3, 5′-GTAGATCAGGTTGGCCAGAAACTC-3′. PCR products were ca. 700 bp (floxed allele, P2 + P3), 600 bp (wild-type allele, P2 + P3), and 400 bp (Δex7 allele, P1 + P3), respectively. The Mck-*cre* transgene was detected by using the forward primer 5′-TCGCGATTATCTTCTATATCTTCAG-3′ and reverse primer 5′-GCTCGACCAGTTTAGTTACCC-3′. Mice were bred and maintained according to institutional guidelines.

Analyses of mRNA, protein expression, and metabolite concentrations. Western blotting was carried out as described previously (6) with antibodies to the C-terminal portion of AIF (AB16501; Chemicon); actin (A-2066; Sigma); cytochrome *c* (Pharmingen); and respiratory chain complex I subunits 39kDa, 30kDa, and 20kDa (all Molecular Probes). For TaqMan real-time PCR analysis of atrial natriuretic factor (ANF) and B-type natriuretic peptide (BNP) expression, 1 μg of DNase-treated total RNA extracted from hearts was reverse transcribed by using oligo(dT). TaqMan reactions were carried out in 96-well plates with 0.5% cDNA, 12.5 μl of 2× TaqMan universal PCR Mastermix, 100 μM probe, 200 μM concentrations of each primer, and water to a final volume of 25 μl. 18S rRNA was used as a control. Blue-native polyacrylamide gel electrophoresis (BN-PAGE) was carried out as described previously (33). Briefly, mitochondria isolated from heart and gastrocnemius were solubilized with extraction buffer containing 1% *n*-dodecyl-maltoside and centrifuged at 100,000 × *g* for 30 min, and the supernatant was analyzed on a 5 to 18% polyacrylamide gradient gel, followed by staining with Coomassie blue. For analysis of plasma metabolite levels, mice were anesthetized with ketamine-xylazine; blood was drawn by cardiac puncture and immediately deproteinated in 1 M perchloric acid. Levels of organic acids, electrolytes, and glucose were determined by conventional methods at the Hôpital Necker-Enfants Malades, Paris, France.

Histological and morphometric analyses. For heart histology, hearts were arrested with 1 M KCl, fixed with 10% buffered formalin, and subsequently embedded in paraffin. Skeletal muscles were snap-frozen in liquid N_2-cooled isopentane, and hematoxylin and eosin and succinic dehydrogenase (SDH) activity stains (26) were performed on cryostat sections. Myocyte areas were quantified by using Oracle imaging software. Samples for electron microscopy were prepared essentially as described previously (18).

Echocardiography and invasive hemodynamic measurements. Echocardiographic and hemodynamic measurements were performed as described previously (6). Briefly, mice were anesthetized with isoflurane(1%)/oxygen, and echocardiographed using an Acuson Sequoia C256 equipped with a 15-MHz linear transducer. Fractional shortening (FS) was calculated as follows: FS = [(EDD − ESD)/EDD] × 100. Vcfc was calculated as FS/ejection time corrected for heart rate. For hemodynamic assessments, the right carotid artery was cannulated with a 1.4 French Millar catheter (Millar, Inc., Houston, TX) connected to an amplifier (TCP-500; Millar, Inc.) After insertion of the catheter into the carotid artery, the catheter was advanced into the aorta and then into the left ventricle to record the aortic and ventricular pressures.

Langendorff perfusion experiments. Mck-*cre*; *Aif*^{flox}/Y mutant and littermate control mice were anesthetized with ketamine-xylazine, and isolated hearts were immediately placed in cold phosphate-buffered saline. Hearts were then perfused in the retrograde Langendorff mode with modified glucose-free, pyruvate-containing Kreb's solution (116 mM NaCl, 3.2 mM KCl, 1.2 mM $MgSO_4$, 25 mM $NaHCO_3$, 1.2 mM KH_2PO_4, 2 mM CaCl, 0.5 mM EDTA, 3 mM sodium pyruvate) in the presence of 95% O_2 and 5% CO_2 to achieve a final pH of 7.4. A pressure transducer balloon was inserted into the left ventricle, and the consequent pressure waveform was recorded at 2 kHz using a Biopac acquisition system. Baseline data was acquired over a 4-min interval. After this period the solution was switched to a pyruvate-free glucose-based Kreb's solution (116 mM NaCl, 3.2 mM KCl, 1.2 mM $MgSO_4$, 25 mM $NaHCO_3$, 1.2 mM KH_2PO_4, 2 mM CaCl, 0.5 mM EDTA, 10 mM glucose), and continuous recordings were obtained for a further 10 min. The temperature was maintained at 36 ± 0.5°C during all recordings.

Assays of mitochondrial function. Mitochondria were prepared by homogenizing heart, skeletal muscle, or liver from Mck-*cre*; *Aif*^{flox}/Y mutant and littermate control mice in homogenization medium (250 mM sucrose, 5 mM Tris-HCl, 2 mM EGTA [pH 7.2]) at 4°C. The homogenate was centrifuged at 760 × *g* for 10 min at 4°C to remove nuclei and cellular debris. The supernatant was then centrifuged at 8,740 × g. The pellet was resuspended in homogenization medium, layered onto a 60%–30%–18% sucrose Percoll gradient, and centrifuged at 8,460 × *g*. Purified mitochondria were washed two times in homogenization buffer. All steps were carried out at 4°C. Rotenone-sensitive NADH quinone reductase (CI; EC 1.6.5.3), malonate-sensitive succinate quinone dichlorophenol indophenol (DCPIP) reductase (CII; EC 1.3.99.1), antimycin-sensitive quinol cytochrome *c* reductase (CIII; EC 1.10.2.2), cyanide-sensitive cytochrome *c* oxidase (CIV; EC1.9.3.1), and oligomycin-sensitive ATP hydrolase (CV; EC 3.6.3.14) were spectrophotometrically measured by using a dual-wavelength spectrophotometer (SLM-Aminco DW-2A; SLM Instruments, Inc., Urbana, IL) as described previously (1, 32). All measurements were performed at 37°C. Protein levels were determined by the method of Bradford with bovine serum albumin as a standard. All chemicals were analytical reagent grade from Sigma Chemical Company.

Lipid peroxidation, catalase activity, and glutathione assays. Lipid peroxidation was analyzed as described previously (30). Catalase activity and total glutathione levels were quantified by using the catalase assay and glutathione assay kits according to the manufacturer's instructions (Cayman Chemicals). Proteins were quantified by using a BCA kit (Pierce).

RESULTS

Generation of tissue-specific AIF mutant mice. To explore the function of AIF, we produced mice carrying a conditional allele of the *Aif*/*Pdcd8* gene, *Aif*^{flox}, by means of gene targeting in ES cells. In this allele, exon 7 (which encodes amino acid residues 232 to 259) of the murine *Aif* gene is flanked by *loxP* sites (Fig. 1A). Cre-mediated excision of exon 7 deletes nucleotides 694 to 778 and disrupts the reading frame. Since *Aif* maps to the X chromosome (36), the targeted XY ES cells

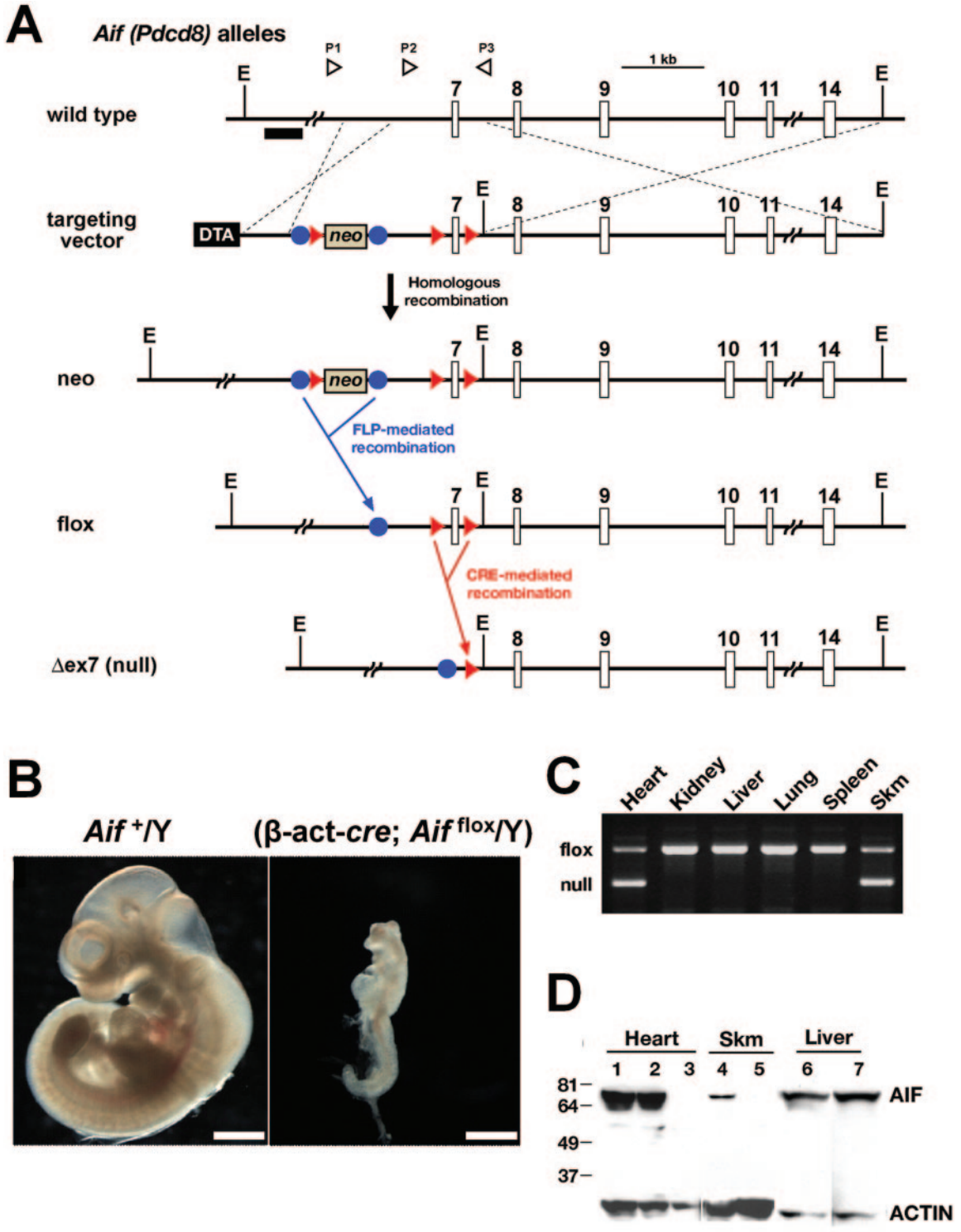

FIG. 1. Conditional inactivation of the mouse *Aif* gene. (A) Partial restriction map of the X-linked mouse *Aif* locus and schematic illustrations of the targeting vector, the modified *Aif* locus after homologous recombination (neo), the *Aif* gene after excision of the *neo* cassette after transient expression of Flp recombinase (flox), and the expected configuration of the mutant *Aif* gene after Cre-mediated excision of exon 7 (Δex7). Exon 7 is flanked by *loxP* sequences (red triangles); the *neo* cassette is flanked by *frt* sequences (blue circles). The 5′ flanking probe used for Southern blots is indicated by a horizontal black bar. The *neo* cassette and diphtheria toxin A (DTA) cassettes are not drawn to scale. The open triangles above the diagram of the wild-type allele indicate the positions of the primers (P1, P2, and P3) used for PCR genotyping. The dotted lines indicate the regions in which homologous recombination occurred. E, EcoRI. (B) By ~E11.0, β-actin-*cre*; Aif^{flox}/Y embryos are markedly reduced in size. A wild-type (Aif^{+}/Y) embryo is shown as an age-matched control. Bar, 1 mm. (C) PCR analysis of tissue-specific recombination at the *Aif* locus in a 1-week-old Mck-*cre*; Aif^{flox}/Y mouse. The Δex7 (null) allele is only present in heart and skeletal muscle (Skm). The presence of a PCR product representing the flox allele in these tissues likely reflects the presence of nonmyocyte cells. (D) Western blot analysis of AIF protein expression in heart, skeletal muscle (skm), and liver from control (lanes 1, 2, 4, and 6) and mutant Mck-*cre*; Aif^{flox}/Y (lanes 3, 5, and 7) mice. Lysates (30 μg) from 13-week-old mice were immunoblotted with anti-AIF and control antiactin antibodies.

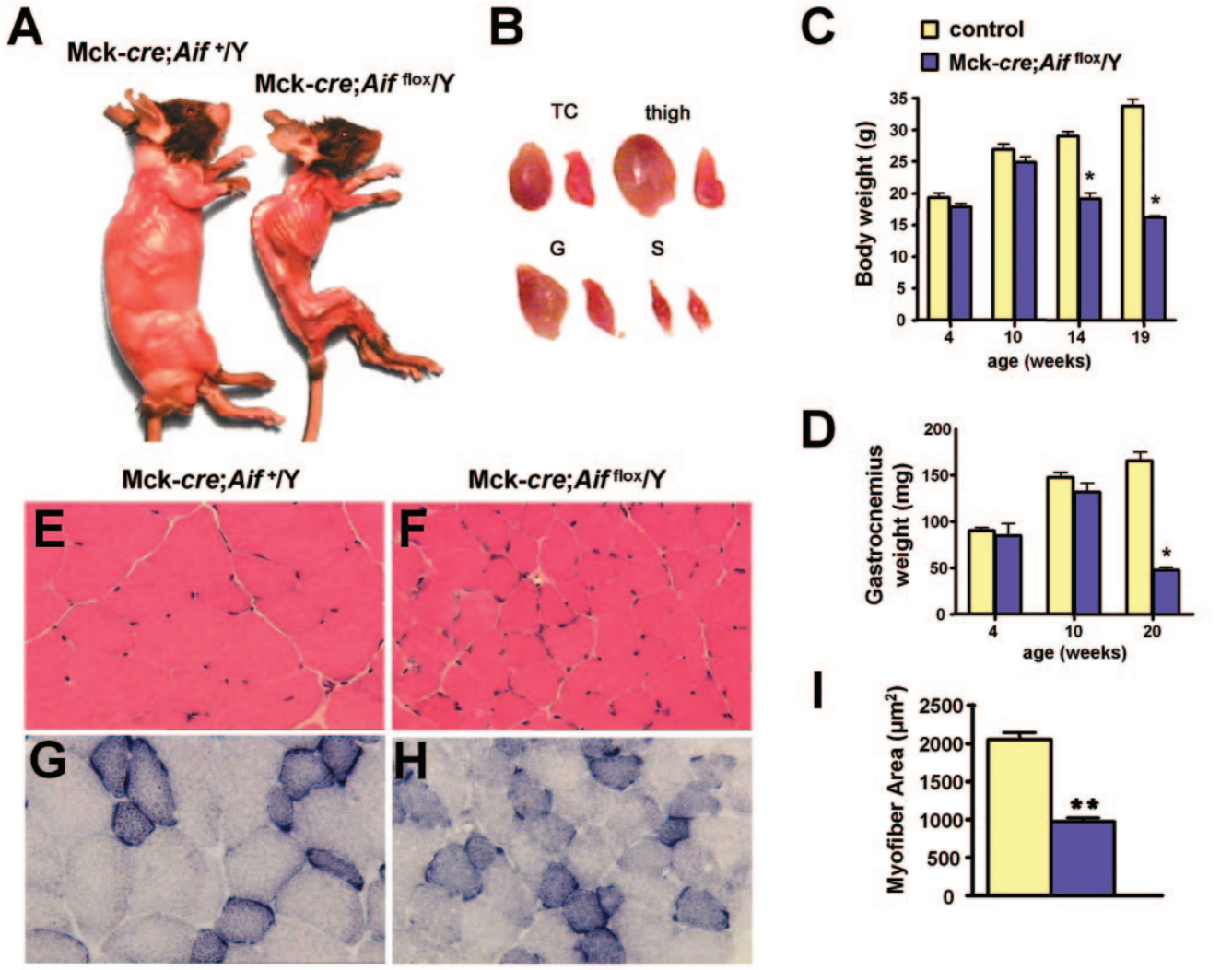

FIG. 2. Progressive skeletal muscle atrophy in Mck-*cre*; *Aif*^{flox}/Y mutant mice. (A) Typical gross morphology of control Mck-*cre*; *Aif*$^{+}$/Y and mutant Mck-*cre*; *Aif*^{flox}/Y mice at 4.5 months of age. (B) Representative pictures of gross morphology of triceps (TC), thigh, gastrocnemius (G), and soleus (S) muscles from (left) control and (right) mutant mice. (C) Body weight measurements for 4-, 10-, 14-, and 19-week-old male Mck-*cre*; *Aif*$^{+}$/Y and mutant Mck-*cre*; *Aif*^{flox}/Y mice. (D) Weight measurements of one gastrocnemius muscle for 4-, 10-, and 20-week-old male Mck-*cre*; *Aif*$^{+}$/Y and mutant Mck-*cre*; *Aif*^{flox}/Y mice. It should be noted that female mutant mice (Mck-*cre*; *Aif*$^{flox/flox}$) have a similar skeletal muscle phenotype. (E and F) Sections of triceps from (E) control and (F) mutant mice stained with hematoxylin and eosin. Magnification, ×300. (G and H) Representative sections of triceps from (G) control and (H) mutant mice stained for SDH activity. Magnification, ×300. (I) Quantitation of myofiber area from triceps of control and mutant mice. Approximately 50 fibers from 2 mice of each genotype were measured by using Oracle software. Mean values ± the standard error of the mean (SEM). *, $P < 0.05$; **, $P < 0.01$ (comparisons between genetic groups [Student's *t* test]).

carry only the mutant *Aif* allele. Two independent *Aif*^{flox}/Y ES cell clones were used to transmit the mutant allele through the germ line (unpublished data). In both lines we observed similar phenotypes throughout the present study.

To analyze the consequences of loss of AIF function in the mouse embryo, we bred *Aif*^{flox}/+ female mice with males homozygous for a β-actin-*cre* transgene that functions to efficiently recombine floxed alleles at preimplantation stages of development (23). In embryos that inherit both *Aif*^{flox} and β-actin-*cre*, the floxed allele is converted to *Aif*$^{\Delta ex7}$, a presumed null allele, early in embryogenesis. Female progeny of this cross that are heterozygous for the *Aif*^{flox} allele (β-actin-*cre*; *Aif*^{flox}/+) are born at lower frequencies than expected for Mendelian inheritance, indicating that some female mutant heterozygotes die in utero. Those that survive to birth are smaller in size than their wild-type littermates but otherwise appear healthy and fertile. In contrast, β-actin-*cre*; *Aif*^{flox}/Y mutant embryos are present at the expected Mendelian frequency between embryonic day 7.5 (E7.5) and E10.5 but exhibit severe growth retardation (Fig. 1B). No viable embryos could be recovered after E12.5 (a detailed analysis of the AIF null phenotype will be described elsewhere.) Thus, complete loss of *Aif* in the early embryo results in a growth arrest and death by E12.5.

Progressive skeletal muscle atrophy in AIF muscle mutant mice. To study the role of AIF in adult tissues that have high energy requirements, we conditionally inactivated *Aif* in cardiac and skeletal muscle by crossing mice carrying *Aif*^{flox} with

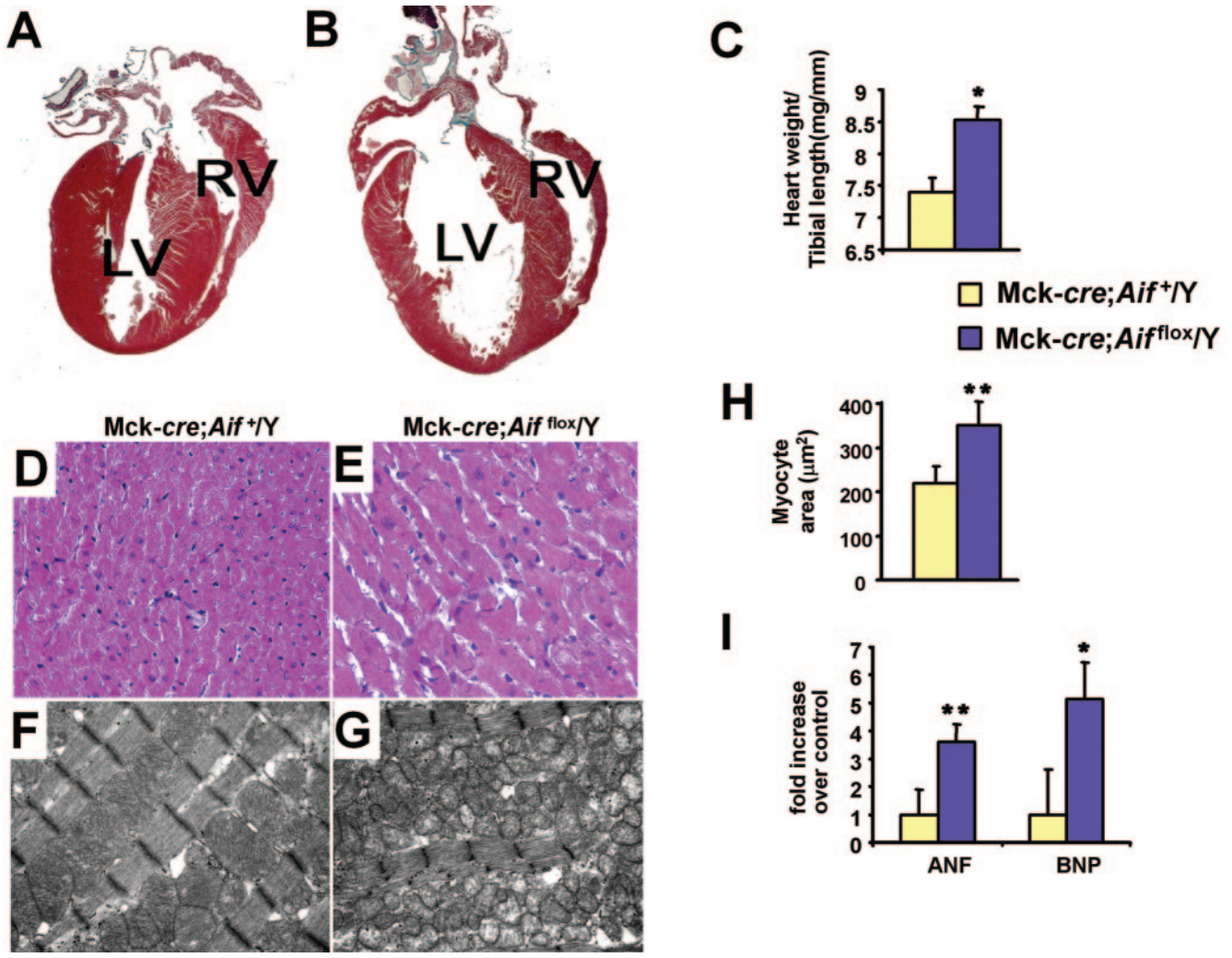

FIG. 3. Dilated cardiomyopathy in Mck-*cre*; *Aif*^{flox}/Y mutant mice. (A and B) Representative heart sections of 9-week-old Mck-*cre*; *Aif*$^{+}$/Y (A) control and Mck-*cre*; *Aif*^{flox}/Y (B) mutant littermates. LV, left ventricle; RV, right ventricle. Masson's trichrome staining was used. (C) Quantitation of heart weight/tibial-length ratios from 9-week-old male control ($n = 7$) and mutant ($n = 7$) littermates. (D and E) Representative heart sections from 9-week-old control (D) and mutant (E) littermates stained with Masson's trichrome. Note the increased cardiomyocyte cell size. Magnification, ×300. (F and G) Electron micrographs of left ventricular heart sections from 13-week-old control (F) and Mck-*cre*; *Aif*^{flox}/Y mutant (G) littermates. Note the abnormal ultrastructure of mitochondria in mutant hearts. Magnification, ×10,000. (H) Increased cell size of cardiomyocytes from 9-week-old control and mutant littermates. A total of 100 individual myocytes from three different mice of each genotype were analyzed per group. (I) Increased mRNA expression (mean ± the SEM) of the cardiac hypertrophy markers ANF and BNP. 18S rRNA was used as a control. The results are from heart tissue isolated from seven control and six mutant littermates at 8 weeks of age. *, $P < 0.01$; **, $P < 0.002$ (for comparisons between genotypes [Student's *t* test]).

a transgenic line expressing *cre* under the control of the muscle creatine kinase promoter (Mck-*cre*). It has been shown previously that this transgene efficiently excises *loxP*-flanked sequences in the heart as well as in all skeletal muscles tested, regardless of anatomical localization or muscle fiber type (2). Crosses of *Aif*^{flox}/+ mice with Mck-*cre* homozygotes produced viable Mck-*cre*; *Aif*^{flox}/Y progeny at the expected Mendelian frequency (~25%). PCR analysis and Western blotting confirmed that *Aif* exon 7 was excised (Fig. 1C and D) and that AIF protein expression was abolished (Fig. 1D) specifically in heart and skeletal muscle tissue from Mck-*cre*; *Aif*^{flox}/Y mutants. As expected, the *Aif* gene did not undergo recombination in other tissues tested (Fig. 1C and D).

Whereas Mck-*cre*; *Aif*^{flox}/Y mutant animals appeared normal at 2 months of age, after 3 months a striking loss in muscle mass and body weight was observed in mutants compared to littermate control mice (Fig. 2A). (Littermate controls used throughout the present study were Mck-*cre*; *Aif*$^{+}$/Y and *Aif*^{flox}/Y mice; no phenotypic differences were observed between these genotypes.) All skeletal muscles analyzed, including triceps, pectoralis, quadriceps, gluteus, and gastrocnemius muscles were significantly atrophied in mutant mice (Fig. 2B). The loss in body weight (Fig. 2C) and degeneration in musculature (Fig. 2D) were progressive, becoming readily detectable after 10 weeks of age. Interestingly, these skeletal muscle changes were more pronounced in predominantly fast-twitch muscles (gas-

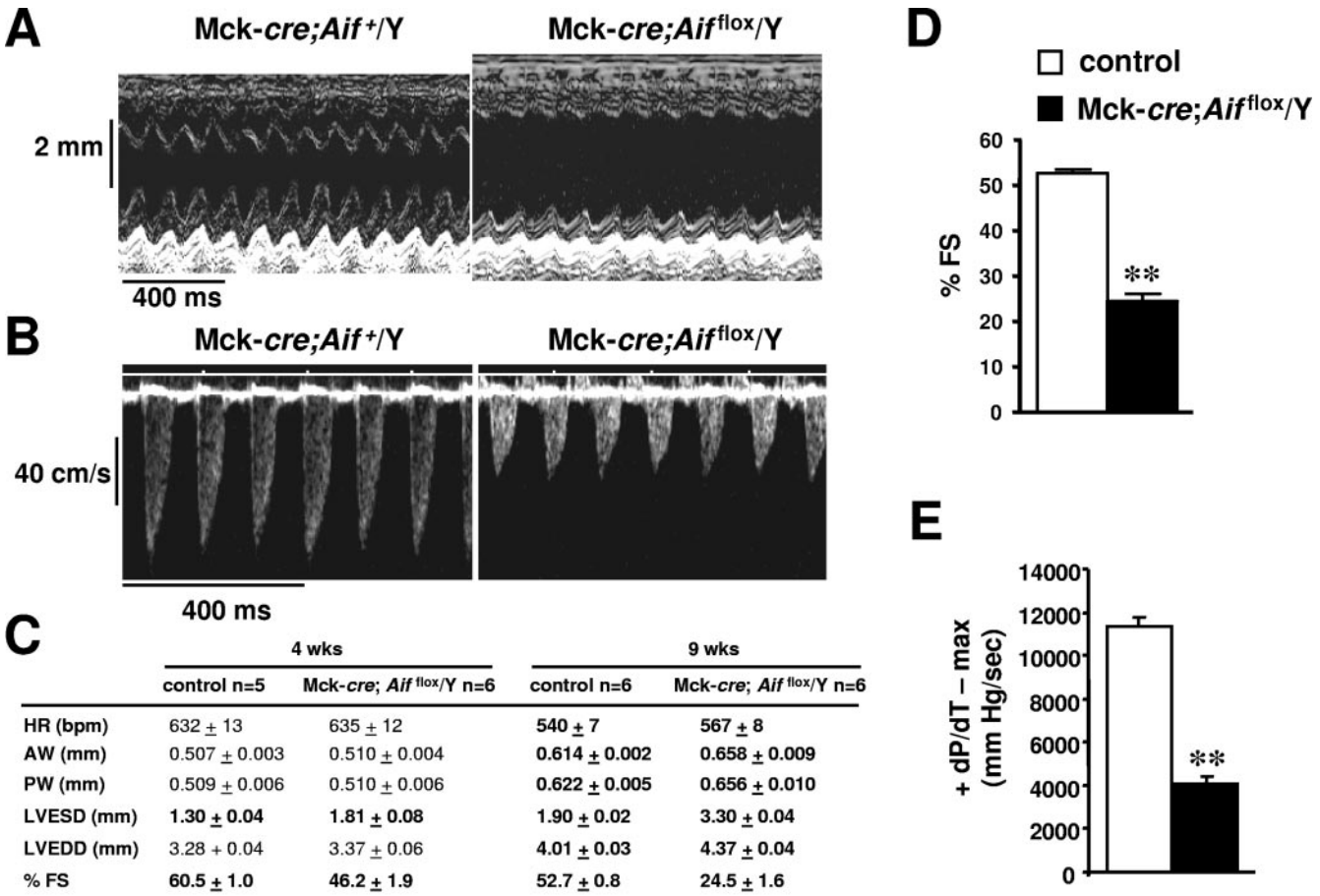

C

	4 wks		9 wks	
	control n=5	Mck-*cre*; *Aif* flox/Y n=6	control n=6	Mck-*cre*; *Aif* flox/Y n=6
HR (bpm)	632 ± 13	635 ± 12	**540 ± 7**	**567 ± 8**
AW (mm)	0.507 ± 0.003	0.510 ± 0.004	**0.614 ± 0.002**	**0.658 ± 0.009**
PW (mm)	0.509 ± 0.006	0.510 ± 0.006	**0.622 ± 0.005**	**0.656 ± 0.010**
LVESD (mm)	**1.30 ± 0.04**	**1.81 ± 0.08**	**1.90 ± 0.02**	**3.30 ± 0.04**
LVEDD (mm)	3.28 + 0.04	3.37 ± 0.06	**4.01 ± 0.03**	**4.37 ± 0.04**
% FS	**60.5 ± 1.0**	**46.2 ± 1.9**	**52.7 ± 0.8**	**24.5 ± 1.6**
PAVc (m/s)	**1.064 ± 0.027**	**0.894 ± 0.029**	**1.058 ± 0.183**	**0.747 ± 0.185**
VCFC (circ/s)	**12.70 ± 0.27**	**9.06 ± 0.28**	**10.81 ± 0.17**	**4.51 ± 0.33**

FIG. 4. Loss of *Aif* results in heart failure. (A) M-mode echocardiographic images of contracting hearts in 9-week-old Mck-*cre*; *Aif*$^{+}$/Y control and Mck-*cre*; *Aif*^{flox}/Y mutant littermates. Representative images are shown. (B) Representative Doppler images of heart contractility in 9-week-old control and mutant littermates. (C) Heart function of 4- and 9-week-old control and mutant littermates. Values were determined by M-mode and Doppler echocardiography. HR, heart rate (beats per minute [bpm]); AW, anterior wall thickness; PW, posterior wall thickness; LVEDD, left ventricle end diastolic dimension; LVESD, left ventricle end systolic dimension; %FS, percent fractional shortening; PAVc, peak aortic outflow velocity; VCFC, velocity of circumferential fiber shortening. Boldface values at 4 weeks indicate $P < 0.01$; boldface values at 9 weeks indicate $P < 0.001$ (Student's *t* test). (D) Percent fractional shortening (%FS) in 9-week-old control and mutant littermates. Values (mean ± the SEM) were determined by echocardiography. (E) +dP/dT-max values in 9-week-old control and mutant littermates. Values (mean ± the SEM) were determined by invasive hemodynamics. In panels D and E, "**" indicates a *P* value of <0.01 between groups (Student's *t* test).

trocnemius, triceps, and quadriceps) compared to the slow-twitch soleus muscle. Atrophy of the skeletal musculature in Mck-*cre*; *Aif*^{flox}/Y mutant mice was accompanied by structural changes. Myofiber cross-sectional area was reduced by >2-fold in triceps of 3-month-old mutant mice compared to those from littermate controls (Fig. 2E, F, and I). Moreover, myofibers in skeletal tissue from 3-month-old mutant mice displayed irregular contours (Fig. 2E and F). Histochemical analysis of muscle tissue sections for SDH activity, an indicator of mitochondrial numbers (13), revealed no obvious abnormalities (Fig. 2G and H). The progressive loss in muscle mass in mutants left the mutant animals increasingly lethargic and, by 5 months of age, they were sacrificed for ethical reasons. Thus, genetic ablation of *Aif* expression in skeletal muscle results in progressively severe deterioration of the skeletal musculature and muscle atrophy.

Loss of AIF in heart muscle results in severe dilated cardiomyopathy. We next explored the consequences of *Aif* inactivation in cardiac muscle. Examination of 9-week-old mice revealed grossly enlarged hearts from Mck-*cre*; *Aif*^{flox}/Y mutant animals compared to their littermate controls (Fig. 3A and B). Concordantly, there was a significant increase in heart weight/tibial-length ratios (Fig. 3C) indicative of cardiac hypertrophy (17). Histological analysis of Mck-*cre*; *Aif*^{flox}/Y mutant animals demonstrated a marked increase in the size of individual cardiomyocytes (Fig. 3D, E, and H). Mutant animals exhibited a significant upregulation of ANF and BNP (Fig. 3I), both prototypical markers of pathological cardiac hypertrophy (12). We did not observe overt differences in cell death in situ, suggesting that loss of *Aif* did not result in altered cardiomyocyte death in vivo (not shown). We next examined the cellular ultrastructure of cardiac muscle from mutant and control mice

TABLE 1. Hemodynamic measurements of control Mck-*cre*; *Aif*$^{+}$/Y and mutant Mck-*cre*; *Aif*^{flox}/Y hearts[a]

Parameter	Mean ± SEM	
	Mck-*cre*; *Aif*$^{+}$/Y ($n = 6$)	Mck-*cre*; *Aif*^{flox}/Y ($n = 6$)
Heart rate (bpm)	536 ± 4	566 ± 11
Systolic BP (mm Hg)	111.8 ± 1.6	87.7 ± 3.2
Diastolic BP (mm Hg)	72.4 ± 1.3	67.6 ± 2.2
Mean arterial BP (mm Hg)	85.6 ± 1.0	74.3 ± 2.4
LVS BP (mm Hg)	110.9 ± 2.1	86.3 ± 3.1
LVED BP (mm Hg)	3.5 ± 0.6	16.2 ± 0.8
$+dP/dt_{max}$ (mm Hg/s)	11,359 ± 405	4,075 ± 344
$-dP/dt_{min}$ (mm Hg/s)	10,983 ± 458	3,457 ± 298

[a] Hemodynamic measurements for 8-week-old mice. bpm, beats per minute; BP, blood pressure; LVS, left ventricular systolic; LVED, left ventricular end diastolic; $+dp/dt_{max}$, maximum first derivative of the change in left ventricular pressure; $-dP/dt_{min}$, minimum first derivative of the change in left ventricular pressure. $P < 0.05$ between genotypes for all comparisons (Student's t test).

TABLE 2. Blood levels of select organic acids

Organic acid	Mean blood level ± SEM[a]	
	Control ($n = 5$)	Mck-*cre*; *Aif*$^{flox/Y}$ ($n = 5$)
Lactate (mmol/liter)	2.3 ± 0.3	5.5 ± 0.5
Pyruvate (mmol/liter)	0.12 ± 0.01	0.15 ± 0.01
Lactate/pyruvate ratio	18.7 ± 2.4	37.2 ± 4.7

[a] Plasma was collected from 13-week-old littermate mice and analyzed for the indicated metabolites. Lactate, $P < 0.001$; pyruvate, $P < 0.02$; L/P, $P < 0.005$.

by using electron microscopy. Whereas wild-type cardiac muscle displayed an orderly myofibrillar architecture and mitochondria with large cristal surface areas (Fig. 3F), mutant heart muscle exhibited pronounced myofibrillar fragmentation and disorganization, as well as increased numbers of mitochondria (Fig. 3G). Moreover, mitochondria from mutant hearts displayed abnormal morphologies and marked cristolysis (Fig. 3G). These quantitative and qualitative changes in mitochondria were not observed in young mutant mice at 4 weeks of age. Thus, genetic inactivation of *Aif* in cardiomyocytes results in the expression of markers indicative of dilated cardiomyopathy.

To further characterize the cardiac abnormalities of mutant Mck-*cre*; *Aif*^{flox}/Y mice, we analyzed cardiac function by echocardiography. Mutant mice exhibited a dramatic reduction in cardiac contractility as evidenced by decreased percent fractional shortening (%FS), decreased velocity of circumferential fiber shortening and markedly reduced peak aortic outflow velocity (Fig. 4A to D). Consistent with the macroscopic and histological examinations of the heart, echocardiography revealed thickening of the ventricular walls and dilation of the left ventricle in mutant animals (Fig. 4C). Furthermore, invasive hemodynamic measurements showed that both dP/dT_{max} and dP/dT_{min} were markedly reduced in *Aif* mutant mice (Fig. 4E and Table 1), indicating severe impairment of contractile heart function. Loss of *Aif* function also resulted in a significant decrease in aortic and ventricular blood pressures (Table 1). Impaired heart function was observed as early as 4 weeks of age and became progressively more severe (Fig. 4C). Importantly, these functional heart defects preceded the changes in mitochondrial ultrastructure (Fig. 3G), indicating that perturbations in mitochondrial structure are secondary to impaired cardiac contractility. These data demonstrate that AIF is required for the maintenance of normal heart function and that loss of *Aif* in cardiomyocytes results in heart failure.

We next determined concentrations of various metabolic intermediates in the plasma of control and Mck-*cre*; *Aif*^{flox}/Y mice. At 13 weeks of age, AIF mutant mice exhibited an ~2.5-fold increase in plasma lactate levels compared to their littermate controls (Table 2). This increase in blood lactate levels was progressive and correlated with the loss in muscle mass (not shown). In mutant mice, a concomitant and significant increase in the lactate/pyruvate ratio was observed. Other blood chemistry parameters analyzed such as glucose and electrolytes such as Ca^{2+} appeared normal in Mck-*cre*; *Aif*^{flox}/Y mice. Elevated blood lactate/pyruvate ratios are commonly observed in patients and mouse mutants with mitochondrial myopathies (13, 28, 41).

Mitochondrial respiratory chain dysfunction and oxidative stress in AIF mutant tissues. The cardiac and skeletal muscle abnormalities and metabolic changes in Mck-*cre*; *Aif*^{flox}/Y mutant mice resemble pathological features observed in humans with disorders in mitochondrial OXPHOS function (9, 21, 29, 39). Moreover, we have recently shown that genetic loss of AIF in embryonic stem cells and downregulation of AIF using RNA interference in cell lines results in compromised respiratory chain function, particularly in the activity and protein expression levels of complex I (37). We therefore determined the respiratory chain competence of heart and skeletal muscle mitochondria from our mutant animals. Measurements of respiratory chain enzyme activities in the predominantly slow-twitch soleus muscle (not shown), fast-twitch gastrocnemius muscle, and heart muscle of Mck-*cre*; *Aif*^{flox}/Y mice revealed a severe (up to 80%) reduction in complex I activity in both skeletal muscle and heart and a milder defect in complex IV activity only in the heart (Fig. 5A). Near-normal or normal activities of complexes II, III, and V were observed. As expected, we found no defect in respiratory chain activities in liver tissue from mutant mice (Fig. 5A). Importantly, these respiratory defects were observed in 5-week-old mice, either preceding or accompanying the development of impaired cardiac function and skeletal muscle atrophy (Fig. 4C and 5B).

To determine whether the observed defect in complex I function was due to a reduction in the expression level of complex I proteins, we resolved and visualized respiratory chain complexes from mitochondria of wild-type and mutant tissues by using BN-PAGE analysis. Consistent with the observed impairment of complex I activity, mutant cardiac and skeletal muscle tissue displayed a significant decrease in protein expression of complex I. In contrast, expression of complexes III, IV, and V were similar between wild-type and mutant tissues (Fig. 5C). Using densitometric analysis and standardizing to complex V levels, complex I expression in mutant hearts was reduced to 50.4% ± 4.2% of control levels; complex III and IV protein levels were 89.5% ± 10.9% and 97.8% ± 0.8% of controls, respectively. In the gastrocnemius, complexes I, III, and IV protein levels from mutant tissue were 50.4% ± 0.3%, 89.8% ± 3.1%, and 104.4% ± 0.7% of control levels, respectively (mean ± the

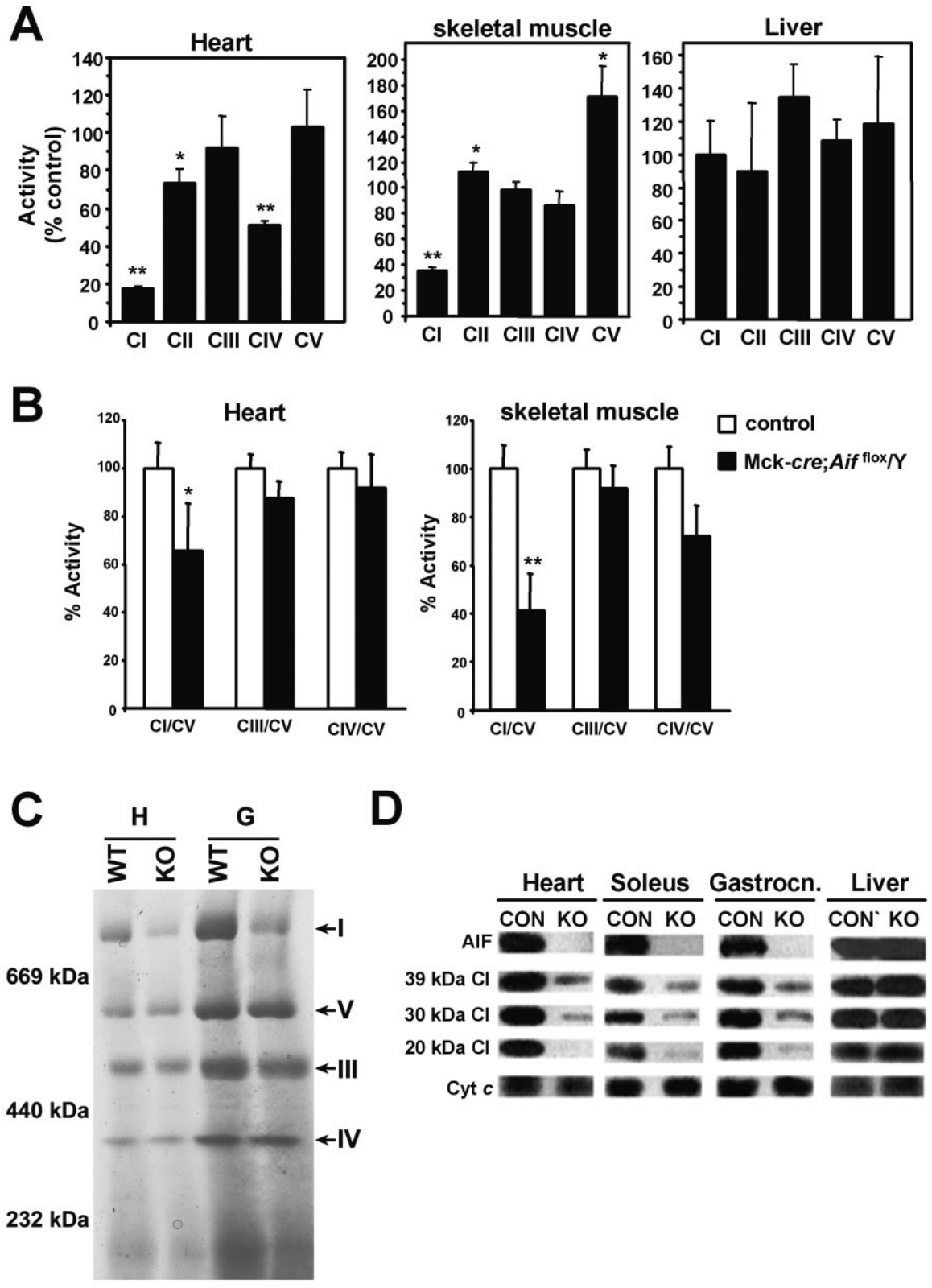

FIG. 5. AIF is required for mitochondrial respiration. (A) Respiratory chain complex activities of mitochondria isolated from heart, skeletal muscle, and liver tissue from 18-week-old control and Mck-*cre*; Aif^{flox}/Y mutant littermates. Shown are relative values of activity (± the SEM) for each complex (I, II, III, IV, and V) of mutant tissues compared to control tissues (100%). *, $P < 0.05$; **, $P < 0.0001$ (B) Respiratory chain complex activities in heart and skeletal muscle from 5-week-old control and Mck-*cre*; Aif^{flox}/Y mutant mice. Relative values of activity (± the SEM) for complexes I, III, and IV normalized to complex V activity and expressed relative to control tissues (100%) are shown. *, $P < 0.05$; **, $P < 0.001$.

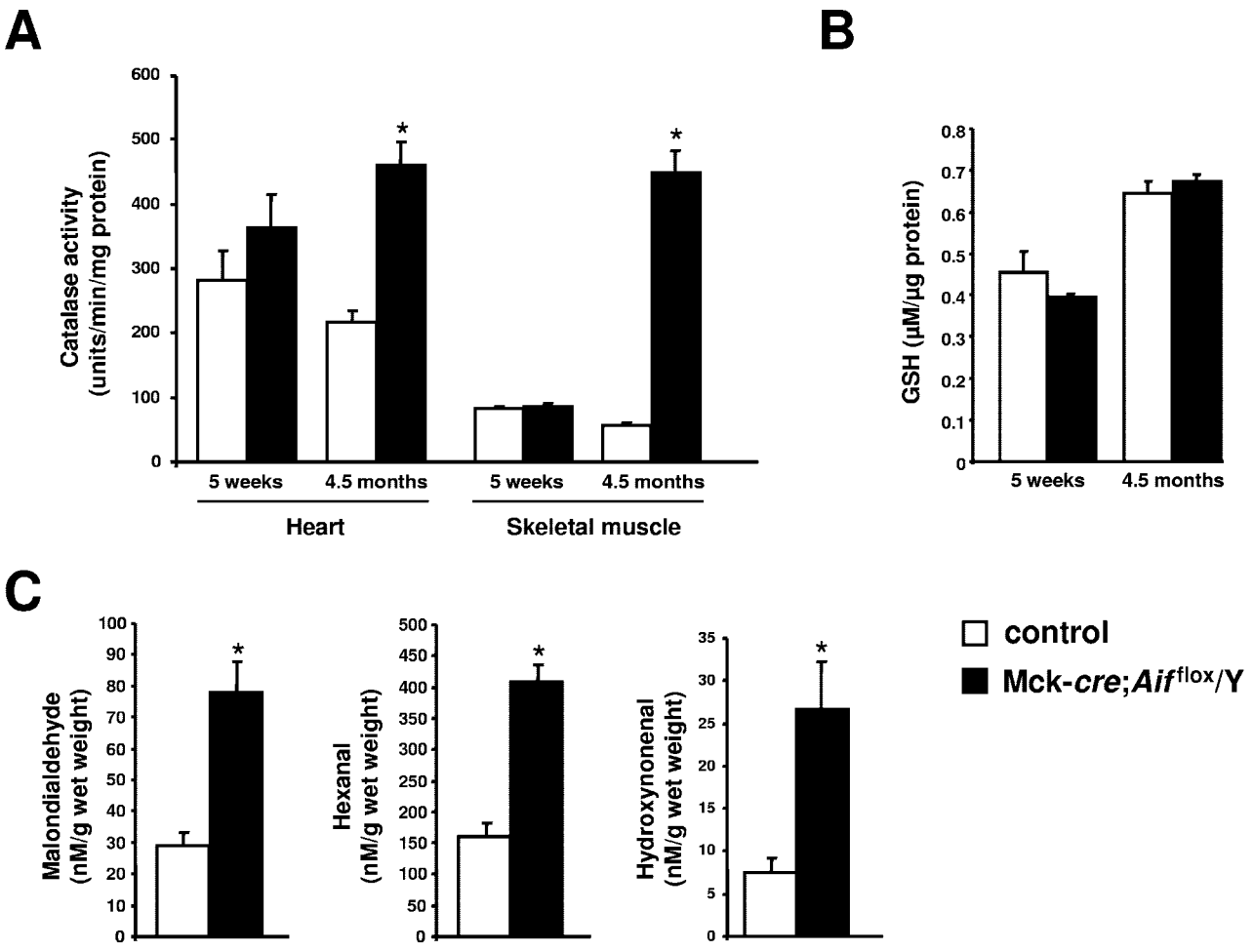

FIG. 6. Increased markers of oxidative stress in mutant tissues. (A) Levels of catalase activity in hearts and thigh muscle (skeletal muscle) from 5-week-old and 4.5-month-old mutant Mck-*cre*; Aif^{flox}/Y and control Mck-*cre*; Aif^{+}/Y mice. Three to five mice were assayed per group. Mean values ± the SEM are shown. *, $P < 0.005$. (B) Total glutathione levels in hearts from 5-week-old and 4.5-month-old mutant Mck-*cre*; Aif^{flox}/Y and control Mck-*cre*; Aif^{+}/Y mice. Mean values ± the SEM are shown. Values between mutant and control samples are not significant. (C) Quantification of lipid peroxidation products malondialdehyde, hexanal, and 4-hydroxynonenal in the hearts of 8-week-old mutant Mck-*cre*; Aif^{flox}/Y and control Mck-*cre*; Aif^{+}/Y mice. Mean values ± the SEM are shown. *, $P < 0.01$. n = six mice assayed per group.

standard deviation; data from three experiments). Furthermore, Western blotting revealed a marked reduction in the level of all complex I subunits tested in the heart, soleus, and gastrocnemius muscles but not in control tissue (Fig. 5D). These data establish in vivo that AIF is required for expression and activity of respiratory chain proteins.

AIF has been previously reported to function as a scavenger of ROS based in part on the observation that neuronal tissue from mice carrying a hypomorphic mutation in *Aif* exhibit high levels of lipid and DNA markers of oxidative stress (20). We quantified the activity of the antioxidant catalase, the principal scavenger of hydrogen peroxide in the cell (8). At 5 weeks of age, hearts and skeletal muscle from mutant and control animals did not exhibit significant differences in levels of catalase activity (Fig. 6A). However, at 4.5 months of age, profound increases in catalase activity were observed in mutant animals compared to controls. Levels of glutathione, an essential electron donor for the reduction of hydroperoxides, were similar between wild-type and mutant hearts (Fig. 6B). Finally, we quantified the levels of lipid peroxidation products malondialdehyde, hexanal, and 4-hydroxynonenal (11). We found that these markers

(C) Diminished expression of respiratory chain complex I in *Aif* mutant tissues from 5-week-old mutant mice. Heart (H) and gastrocnemius (G) muscle mitochondria from wild-type (WT) and Mck-*cre*; Aif^{flox}/Y (KO) mice were subjected to BN-PAGE to resolve respiratory chain complexes. Arrows indicate complexes I, III, IV, and V. (D) Abrogated expression of respiratory chain complex I (CI) subunits in the heart, gastrocnemius, and soleus muscles from Mck-*cre*; Aif^{flox}/Y mutant mice compared to Mck-*cre*; Aif^{+}/Y control mice. Tissue lysates from 18-week-old mice were subjected to Western blotting. Liver tissue was used as a control. Cytochrome *c* (Cyt *c*) expression is shown as a loading control.

A

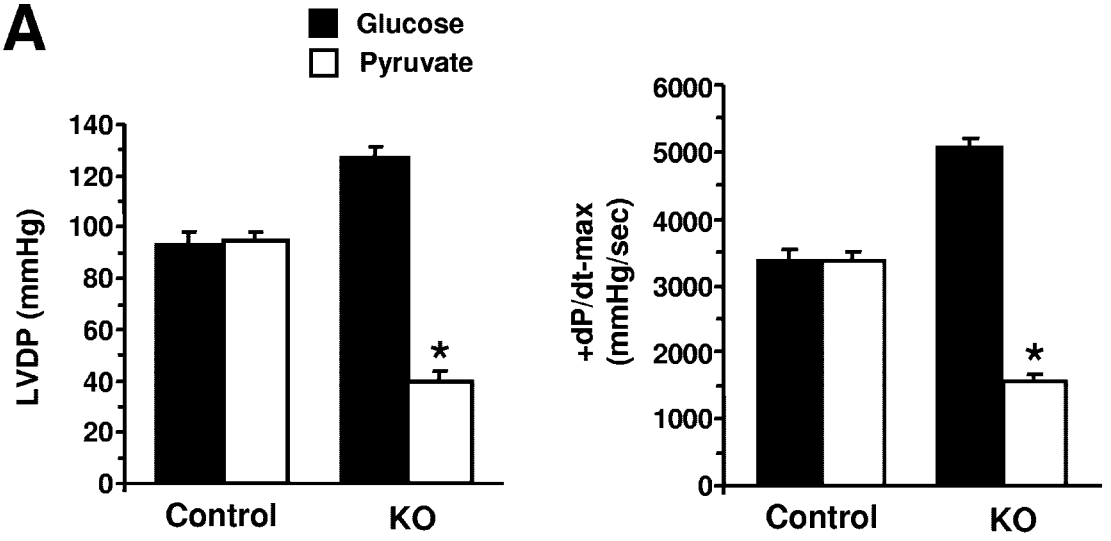

B

	Pyruvate (3 mM)		Glucose (10 mM)	
	Mck-cre;*Aif* $^{+}$/Y	Mck-cre;*Aif* ^{flox}/Y	Mck-cre;*Aif* $^{+}$/Y	Mck-cre;*Aif* ^{flox}/Y
HR (bpm)	394±9.7	228±14.3*	389±9.8	345±13#
LVEDP (mmHg)	5.08±1.12	7.98±0.64	4.94±1.14	0.29±1.18#
LVSP (mmHg)	100.3±2.7	47.6±3.9*	98.1±5.2	127.3±4.2#
LVDP (mmHg)	94.8±2.9	39.6±4.1*	93.1±4.7	127±3.9#
+dP/dtmax (mmHg/sec)	3375±132	1557±106*	3352±171	5061±129#
-dP/dtmin (mmHg/sec)	3209±100	1302±103*	3122±115	4308±141#

FIG. 7. AIF mutant hearts undergo a metabolic switch toward glycolysis. (A and B) Ex vivo heart function of control and mutant (KO) littermates perfused with pyruvate or glucose. HR, heart rate (in beats per minute [bpm]); LVEDP, left ventricular end diastolic pressure; LVSP, left ventricular systolic pressure; LVDP, left ventricular developed pressure; LVDP, LVSP-LVEDP; +dP/dtmax, maximum first derivative of the change in left ventricular pressure; −dP/dtmin, minimum first derivative of the change in left ventricular pressure. Values are means ± the SEM are shown. Male *Aif* knockouts and littermate controls at 9 weeks of age were analyzed. n = five per group. *, $P < 0.01$ compared to all other groups; #, $P < 0.01$ compared to mutant hearts perfused with pyruvate.

were elevated >2.5-fold in the hearts of 9-week-old Mck-*cre*; *Aif*^{flox}/Y mutant mice compared to control littermates (Fig. 6C). Thus, loss of AIF results in increased levels of some markers of oxidative stress and impaired mitochondrial respiration.

Mutant hearts undergo a metabolic switch toward glucose metabolism. Mice with defects in mitochondrial respiration have been shown to switch their metabolism away from fatty acid oxidation and toward glycolysis (15). We investigated whether Mck-*cre*; *Aif*^{flox}/Y mutant hearts metabolically switch their energy substrate preferences toward glucose. To address this, we subjected hearts from wild-type and Mck-*cre*; *Aif*^{flox}/Y mutant mice to Langendorff perfusion, assessing ex vivo heart function under defined fuel substrate conditions. When pyruvate, a fuel efficiently utilized only by cells with a functioning respiratory chain, was the sole carbon source in the perfusion medium, mutant hearts exhibited severe hemodynamic and contractile abnormalities, as had been observed in vivo. All functional heart parameters, such as dP/dT_{max} and dP/dT_{min}, indicative of generated contractile pressure were markedly reduced in mutant hearts perfused with pyruvate (Fig. 7A and B). However, when glucose was used as fuel substrate in the perfusion medium, mutant hearts strikingly improved their contractile performance and even exhibited increased contractility compared to wild-type hearts (Fig. 7A and B). These results suggest that *Aif* mutant cardiomyocytes undergo a compensatory metabolic switch toward glucose utilization and glycolysis and support the notion that AIF plays an essential role in mitochondrial respiration and energy homeostasis.

DISCUSSION

We have shown recently that genetic loss of AIF in ES cells and downregulation of AIF by using RNA interference in cell lines result in enhanced dependency on glycolysis for ATP production due to a severe reduction in complex I activity (37). We also demonstrated diminished complex I function in the brain and retina of Harlequin mice, which manifest an ~80% reduction in AIF protein levels and exhibit late-onset ataxia and degeneration of retinal and cerebellar neurons (20, 37). In the present study, we extend these findings into mice carrying a null allele of the *Aif* gene. We show that loss of AIF during embryogenesis results in growth arrest and death by E12.5. It seems likely that the phenotype results from defects in mitochondrial respiration, since we show that inactivation of AIF in heart and skeletal muscle leads to compromised complex I function in these tissues. Moreover, mutation of genes encoding components of the respiratory chain or regulating mitochondrial respiration leads to early embryonic growth retardation and lethality (22, 24).

We demonstrate further that AIF is required for the maintenance of normal heart and skeletal muscle function. Inactivation of AIF in these tissues results in dilated cardiomyopathy, progressive muscle atrophy and weakness, and lactic acidemia. This physiological and metabolic profile resembles characteristics of mitochondrial myopathies and cardiomyopathies from patients with defects in OXPHOS (39, 40). Such alterations are also observed in genetically altered mutant mice with primary OXPHOS defects (13, 21, 41). For example, mice carrying a mutation in the gene encoding the muscle isoform of adenine nucleotide translocator (ANT1) develop cardiac hypertrophy with mitochondrial proliferation, elevated serum lactate levels, and muscle fatigue after exercise (13). It is noteworthy that we did not observe in our mutant mice ragged-red muscle fibers (Fig. 2G and H), which are indicative of mitochondrial proliferation and are observed in some other mouse models of mitochondrial myopathies (13, 44). This discrepancy may relate to the fact that the respiratory defect in our mutants is more limited, affecting predominantly complex I, than in these other mutant mouse models. Our data point to a role for AIF in mitochondrial respiration and energy metabolism essential for normal tissue function.

It has been suggested previously that AIF controls the cellular redox state by functioning as a scavenger of free radicals (19, 20). In support of this, cerebellar and retinal neurons from the Harlequin (*Hq*) mouse exhibit increased oxidative stress and cerebellar granule cells display increased sensitivity to hydrogen peroxide-mediated cell death in culture (20). Recently, it has been shown that hearts from *Hq* mice exhibit more severe tissue damage after acute ischemia-reperfusion injury and *Hq* cardiomyocytes are sensitized to oxidative stress-induced cell death (38). In line with these findings, our muscle-specific AIF mutants displayed elevated levels of oxidative stress, including increased catalase activity and lipid peroxidation. Since defects in respiratory chain function can result in increased oxidative stress (10) and in light of our data demonstrating defects in complex I function in *Aif* mutant mice, we suggest an alternative interpretation of the *Hq* phenotype, namely, that the primary defect resulting from loss of AIF expression is impaired mitochondrial respiration, which then leads to the observed upregulation of oxidative stress markers. Moreover, if impaired OXPHOS were secondary to increased oxidative stress, then one might expect to see more generalized defects in complexes I, II, and III, as are observed in genetically altered mice carrying mutations in antioxidant defense genes, such as the SOD2 and frataxin knockout mice (27, 31). However, such generalized defects were not observed in our mutant animals. Although we cannot exclude a role for AIF as an antioxidant, we favor the notion of a primary role for AIF in regulating mitochondrial respiration. Indeed, neuronal degeneration is frequently observed in patients and animal models with defective OXPHOS (21).

In addition to a complex I functional defect in our AIF mutant animals, we observed milder defects in complex IV activity, particularly in the heart. This may result from destabilization of the postulated I/III/IV supercomplex subsequent to defects in complex I (34). The mechanism by which AIF regulates mitochondrial respiration through complex I (and possibly other respiratory complexes) remains to be determined. AIF does not interact with complex I nor does loss of AIF affect transcription of complex I subunits (37). Since AIF-deficient tissues exhibit a reduced content of complex I and its components, AIF may play a role in the biogenesis and/or stability of the complex. Very little is known of the mechanism of complex I assembly, and only one assembly factor has been identified in mammals (35). The redox activity of AIF might play a role in controlling the redox status of one key component of complex I, either necessary for the correct assembly/maintenance of the complex or for normal electron transfer through the complex.

AIF was originally characterized as a caspase-independent apoptogenic molecule and has since been shown to participate and, in some cases, to be required in multiple systems of cell death. For instance, knockdown of *Aif* expression in *Caenorhabditis elegans* using RNA interference prolonged duration of development as a result of inefficient programmed cell death (42). Cortical neurons from *Hq* mice as well as *Aif*-null murine ES cells exhibited partial resistance to cell death after serum withdrawal (18, 20). This apparent functional duality of AIF underscores the notion that the apparatus involved in the suicide of a cell is intimately linked to basic cellular life-sustaining processes.

ACKNOWLEDGMENTS

We are indebted to A. Pospisilik, B. McManus, B. Dickson, R. Khokha, and G. R. Martin for helpful discussions and critical reading of the manuscript. We thank R. Sarao, L. Morikawa, and D. Holmyard for help with histological analyses.

This study was supported by grants from IMBA, the Austrian National Bank Jubilaeumsfonds, and the Austrian Academy of Sciences (to J.M.P.); grants from LNC, EU, and Ministere pour la Recherche (to G.K.); and an Ontario Graduate Scholarship (to N.J.) and an ARC fellowship (N.V.). P.H.B. and P.R. thank the Association Française contre les Myopathies and the Association contre les Maladies Mitochondriales for their constant support.

REFERENCES

1. **Benit, P., A. Slama, F. Cartault, I. Giurgea, D. Chretien, S. Lebon, C. Marsac, A. Munnich, A. Rotig, and P. Rustin.** 2004. Mutant NDUFS3 subunit of mitochondrial complex I causes Leigh syndrome. J. Med. Genet. **41:**14–17.
2. **Bruning, J. C., M. D. Michael, J. N. Winnay, T. Hayashi, D. Horsch, D. Accili, L. J. Goodyear, and C. R. Kahn.** 1998. A muscle-specific insulin

receptor knockout exhibits features of the metabolic syndrome of NIDDM without altering glucose tolerance. Mol. Cell **2:**559–569.
3. **Buchholz, F., P. O. Angrand, and A. F. Stewart.** 1998. Improved properties of FLP recombinase evolved by cycling mutagenesis. Nat. Biotechnol. **16:** 657–662.
4. **Budihardjo, I., H. Oliver, M. Lutter, X. Luo, and X. Wang.** 1999. Biochemical pathways of caspase activation during apoptosis. Annu. Rev. Cell Dev. Biol. **15:**269–290.
5. **Chomyn, A., and G. Attardi.** 2003. MtDNA mutations in aging and apoptosis. Biochem. Biophys. Res. Commun. **304:**519–529.
6. **Crackower, M. A., G. Y. Oudit, I. Kozieradzki, R. Sarao, H. Sun, T. Sasaki, E. Hirsch, A. Suzuki, T. Shioi, J. Irie-Sasaki, R. Sah, H. Y. Cheng, V. O. Rybin, G. Lembo, L. Fratta, A. J. Oliveira-dos-Santos, J. L. Benovic, C. R. Kahn, S. Izumo, S. F. Steinberg, M. P. Wymann, P. H. Backx, and J. M. Penninger.** 2002. Regulation of myocardial contractility and cell size by distinct PI3K-PTEN signaling pathways. Cell **110:**737–749.
7. **Danial, N. N., and S. J. Korsmeyer.** 2004. Cell death: critical control points. Cell **116:**205–219.
8. **Deisseroth, A., and A. L. Dounce.** 1970. Catalase: physical and chemical properties, mechanism of catalysis, and physiological role. Physiol. Rev. **50:**319–375.
9. **DiMauro, S., and E. A. Schon.** 2003. Mitochondrial respiratory-chain diseases. N. Engl. J. Med. **348:**2656–2668.
10. **Esposito, L. A., S. Melov, A. Panov, B. A. Cottrell, and D. C. Wallace.** 1999. Mitochondrial disease in mouse results in increased oxidative stress. Proc. Natl. Acad. Sci. USA **96:**4820–4825.
11. **Esterbauer, H., R. J. Schaur, and H. Zollner.** 1991. Chemistry and biochemistry of 4-hydroxynonenal, malonaldehyde and related aldehydes. Free Radic. Biol. Med. **11:**81–128.
12. **Frey, N., and E. N. Olson.** 2003. Cardiac hypertrophy: the good, the bad, and the ugly. Annu. Rev. Physiol. **65:**45–79.
13. **Graham, B. H., K. G. Waymire, B. Cottrell, I. A. Trounce, G. R. MacGregor, and D. C. Wallace.** 1997. A mouse model for mitochondrial myopathy and cardiomyopathy resulting from a deficiency in the heart/muscle isoform of the adenine nucleotide translocator. Nat. Genet. **16:**226–234.
14. **Green, D. R., and J. C.** 1998. Reed mitochondria and apoptosis. Science **281:**1309–1312.
15. **Hansson, A., N. Hance, E. Dufour, A. Rantanen, K. Hultenby, D. A. Clayton, R. Wibom, and N. G. Larsson.** 2004. A switch in metabolism precedes increased mitochondrial biogenesis in respiratory chain-deficient mouse hearts. Proc. Natl. Acad. Sci. USA **101:**3136–3141.
16. **Hooper, M., K. Hardy, A. Handyside, S. Hunter, and M. Monk.** 1987. HPRT-deficient (Lesch-Nyhan) mouse embryos derived from germline colonization by cultured cells. Nature **326:**292–295.
17. **Hunter, J. J., and K. R. Chien.** 1999. Signaling pathways for cardiac hypertrophy and failure. N. Engl. J. Med. **341:**1276–1283.
18. **Joza, N., S. A. Susin, E. Daugas, W. L. Stanford, S. K. Cho, C. Y. Li, T. Sasaki, A. J. Elia, H. Y. Cheng, L. Ravagnan, K. F. Ferri, N. Zamzami, A. Wakeham, R. Hakem, H. Yoshida, Y. Y. Kong, T. W. Mak, J. C. Zuniga-Pflucker, G. Kroemer, and J. M. Penninger.** 2001. Essential role of the mitochondrial apoptosis-inducing factor in programmed cell death. Nature **410:**549–554.
19. **Klein, J. A., and S. L. Ackerman.** 2003. Oxidative stress, cell cycle, and neurodegeneration. J. Clin. Investig. **111:**785–793.
20. **Klein, J. A., C. M. Longo-Guess, M. P. Rossmann, K. L. Seburn, R. E. Hurd, W. N. Frankel, R. T. Bronson, and S. L. Ackerman.** 2002. The harlequin mouse mutation downregulates apoptosis-inducing factor. Nature **419:**367–374.
21. **Larsson, N. G., and P. Rustin.** 2001. Animal models for respiratory chain disease. Trends Mol. Med. **7:**578–581.
22. **Larsson, N. G., J. Wang, H. Wilhelmsson, A. Oldfors, P. Rustin, M. Lewandoski, G. S. Barsh, and D. A. Clayton.** 1998. Mitochondrial transcription factor A is necessary for mtDNA maintenance and embryogenesis in mice. Nat. Genet. **18:**231–236.
23. **Lewandoski, M., E. N. Meyers, and G. R. Martin.** 1997. Analysis of Fgf8 gene function in vertebrate development. Cold Spring Harbor Symp. Quant. Biol. **62:**159–168.
24. **Li, K., Y. Li, J. M. Shelton, J. A. Richardson, E. Spencer, Z. J. Chen, X. Wang, and R. S. Williams.** 2000. Cytochrome *c* deficiency causes embryonic lethality and attenuates stress-induced apoptosis. Cell **101:**389–399.
25. **Loeffler, M., E. Daugas, S. A. Susin, N. Zamzami, D. Metivier, A. L. Nieminen, G. Brothers, J. M. Penninger, and G. Kroemer.** 2001. Dominant cell death induction by extramitochondrially targeted apoptosis-inducing factor. FASEB J. **15:**758–767.
26. **Lojda, Z., R. Gossrau, and T. H. Schiebler.** 1979. Enzyme histochemistry: a laboratory manual. Springer-Verlag, New York, N.Y.
27. **Melov, S., P. Coskun, M. Patel, R. Tuinstra, B. Cottrell, A. S. Jun, T. H. Zastawny, M. Dizdaroglu, S. I. Goodman, T. T. Huang, H. Miziorko, C. J. Epstein, and D. C. Wallace.** 1999. Mitochondrial disease in superoxide dismutase 2 mutant mice. Proc. Natl. Acad. Sci. USA **96:**846–851.
28. **Munnich, A., A. Rotig, D. Chretien, J. M. Saudubray, V. Cormier, and P. Rustin.** 1996. Clinical presentations and laboratory investigations in respiratory chain deficiency. Eur. J. Pediatr. **155:**262–274.
29. **Munnich, A., and P. Rustin.** 2001. Clinical spectrum and diagnosis of mitochondrial disorders. Am. J. Med. Genet. **106:**4–17.
30. **Oudit, G. Y., H. Sun, M. G. Trivieri, S. E. Koch, F. Dawood, C. Ackerley, M. Yazdanpanah, G. J. Wilson, A. Schwartz, P. P. Liu, and P. H. Backx.** 2003. L-type Ca^{2+} channels provide a major pathway for iron entry into cardiomyocytes in iron-overload cardiomyopathy. Nat. Med. **9:**1187–1194.
31. **Rotig, A., P. de Lonlay, D. Chretien, F. Foury, M. Koenig, D. Sidi, A. Munnich, and P. Rustin.** 1997. Aconitase and mitochondrial iron-sulphur protein deficiency in Friedreich ataxia. Nat. Genet. **17:**215–217.
32. **Rustin, P., D. Chretien, T. Bourgeron, B. Gerard, A. Rotig, J. M. Saudubray, and A. Munnich.** 1994. Biochemical and molecular investigations in respiratory chain deficiencies. Clin. Chim Acta **228:**35–51.
33. **Schagger, H.** 2001. Blue-native gels to isolate protein complexes from mitochondria. Methods Cell Biol. **65:**231–244.
34. **Schagger, H.** 2002. Respiratory chain supercomplexes of mitochondria and bacteria. Biochim. Biophys. Acta **1555:**154–159.
35. **Schulte, U.** 2001. Biogenesis of respiratory complex I. J. Bioenerg. Biomembr. **33:**205–212.
36. **Susin, S. A., H. K. Lorenzo, N. Zamzami, I. Marzo, B. E. Snow, G. M. Brothers, J. Mangion, E. Jacotot, P. Costantini, M. Loeffler, N. Larochette, D. R. Goodlett, R. Aebersold, D. P. Siderovski, J. M. Penninger, and G. Kroemer.** 1999. Molecular characterization of mitochondrial apoptosis-inducing factor. Nature **397:**441–446.
37. **Vahsen, N., C. Cande, J. J. Briere, P. Benit, N. Joza, N. Larochette, P. G. Mastroberardino, M. O. Pequignot, N. Casares, V. Lazar, O. Feraud, N. Debili, S. Wissing, S. Engelhardt, F. Madeo, M. Piacentini, J. M. Penninger, H. Schagger, P. Rustin, and G. Kroemer.** 2004. AIF deficiency compromises oxidative phosphorylation. EMBO J. **23:**4679–4689.
38. **van Empel, V. P., A. T. Bertrand, R. van der Nagel, S. Kostin, P. A. Doevendans, H. J. Crijns, E. de Wit, W. Sluiter, S. L. Ackerman, and L. J. De Windt.** 2005. Downregulation of apoptosis-inducing factor in harlequin mutant mice sensitizes the myocardium to oxidative stress-related cell death and pressure overload-induced decompensation. Circ. Res. **96:**e92–e101.
39. **Wallace, D. C.** 1999. Mitochondrial diseases in man and mouse. Science **283:**1482–1488.
40. **Wallace, D. C.** 1997. Mitochondrial DNA in aging and disease. Sci. Am. **277:**40–47.
41. **Wang, J., H. Wilhelmsson, C. Graff, H. Li, A. Oldfors, P. Rustin, J. C. Bruning, C. R. Kahn, D. A. Clayton, G. S. Barsh, P. Thoren, and N. G. Larsson.** 1999. Dilated cardiomyopathy and atrioventricular conduction blocks induced by heart-specific inactivation of mitochondrial DNA gene expression. Nat. Genet. **21:**133–137.
42. **Wang, X., C. Yang, J. Chai, Y. Shi, and D. Xue.** 2002. Mechanisms of AIF-mediated apoptotic DNA degradation in *Caenorhabditis elegans*. Science **298:**1587–1592.
43. **Wissing, S., P. Ludovico, E. Herker, S. Buttner, S. M. Engelhardt, T. Decker, A. Link, A. Proksch, F. Rodrigues, M. Corte-Real, K. U. Frohlich, J. Manns, C. Cande, S. J. Sigrist, G. Kroemer, and F. Madeo.** 2004. An AIF orthologue regulates apoptosis in yeast. J. Cell Biol. **166:**969–974.
44. **Wredenberg, A., R. Wibom, H. Wilhelmsson, C. Graff, H. H. Wiener, S. J. Burden, A. Oldfors, H. Westerblad, and N. G. Larsson.** 2002. Increased mitochondrial mass in mitochondrial myopathy mice. Proc. Natl. Acad. Sci. USA **99:**15066–15071.